

SGLC: Semantic Graph-Guided Coarse-Fine-Refine Full Loop Closing for LiDAR SLAM

Neng Wang*, Xieyuanli Chen*, Chenghao Shi, Zhiqiang Zheng, Hongshan Yu, Huimin Lu[†]

Abstract—Loop closing is a crucial component in SLAM that helps eliminate accumulated errors through two main steps: loop detection and loop pose correction. The first step determines whether loop closing should be performed, while the second estimates the 6-DoF pose to correct odometry drift. Current methods mostly focus on developing robust descriptors for loop closure detection, often neglecting loop pose estimation. A few methods that do include pose estimation either suffer from low accuracy or incur high computational costs. To tackle this problem, we introduce SGLC, a real-time semantic graph-guided full loop closing method, with robust loop closure detection and 6-DoF pose estimation capabilities. SGLC takes into account the distinct characteristics of foreground and background points. For foreground instances, it builds a semantic graph that not only abstracts point cloud representation for fast descriptor generation and matching but also guides the subsequent loop verification and initial pose estimation. Background points, meanwhile, are exploited to provide more geometric features for scan-wise descriptor construction and stable planar information for further pose refinement. Loop pose estimation employs a coarse-fine-refine registration scheme that considers the alignment of both instance points and background points, offering high efficiency and accuracy. We evaluate the loop closing performance of SGLC through extensive experiments on the KITTI and KITTI-360 datasets, demonstrating its superiority over existing state-of-the-art methods. Additionally, we integrate SGLC into a SLAM system, eliminating accumulated errors and improving overall SLAM performance. The implementation of SGLC will be released at <https://github.com/nubot-nudt/SGLC>.

Index Terms—Semantic Graph, Loop Closing, LiDAR SLAM

I. INTRODUCTION

Loop closing plays a crucial role in simultaneous localization and mapping (SLAM) systems for correcting odometry drifts and building consistent maps, especially in single-sensor SLAM without GPS information. LiDAR-based loop closing typically requires feature extraction from LiDAR scans to generate discriminative descriptors. This task is especially challenging due to the extensive and sparse nature of point clouds in outdoor operations for autonomous robots.

While many existing methods [1]–[6] focus on loop closure detection (LCD), few can estimate closed-loop pose in six degrees of freedom (6-DoF). Some methods incorporate pose estimation with 1-DoF [7]–[9] or 3-DoF [10], which may

N. Wang, X. Chen, C. Shi, Z. Zheng and H. Lu are with the College of Intelligence Science and Technology, National University of Defense Technology. H. Yu is with the Hunan University.

* indicate equal contribution. [†]corresponding author, lhmnew@nudt.edu.cn.

This work was supported in part by the National Science Foundation of China under Grant U1913202, U22A2059, and 62203460, Young Elite Scientists Sponsorship Program by CAST (No. 2023QNRC001), as well as Major Project of Natural Science Foundation of Hunan Province under Grant 2021JC0004.

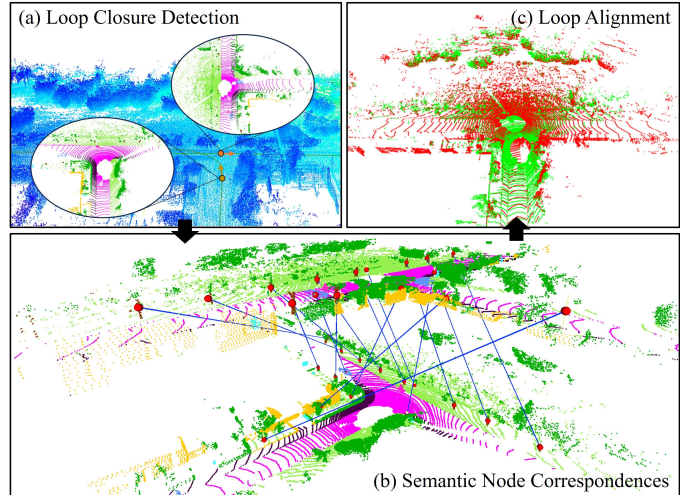


Fig. 1: Visualization of loop closing using our method. (a) Loop closure detection, it shows a reverse loop on the KITTI 08 sequence found by our approach even with significant changes in the position and orientation. (b) Semantic node correspondences for geometric verification and initial loop poses estimation. The blue lines indicate the node correspondences and red spheres represent the estimated instance center. (c) Final alignment for loop correction.

not be sufficient for 6-DoF SLAM systems. Exiting full 6-DoF pose estimation methods, however, are either very time-consuming [11] or have relatively lower accuracy [12].

To tackle these issues, we propose SGLC, an efficient semantic graph-guided full loop closing framework that offers both robust LCD and accurate 6-DoF loop pose estimation. Different from existing semantic graph-based methods [3], [13] that indiscriminately use both foreground instances and background points, or those overlook the geometrically rich background point clouds [14], our method leverages the distinct properties of both foreground and background elements efficiently. SGLC builds semantic graphs based on foreground instances as they can be naturally represented as individual nodes. While for retrieving loop candidates and estimating 6-DoF poses, SGLC exploits both the topological properties of the semantic graph and the geometric features of background points to enhance loop closing accuracy and robustness.

Specifically, SGLC first generates LiDAR scan descriptors to quickly retrieve multiple candidate scans by exploiting the semantics and typologies of the foreground semantic graph and the geometric features of the background. To prevent incorrect loops from compromising the SLAM system, we apply geometric verification to eliminate false loop candidates by identifying graph node correspondences between the query

and candidate scans. During node matching, we ensure accurate correspondences and facilitate the process through an outlier correspondence pruning method based on their neighbor geometric structure. Finally, for the verified loop candidate scan, we propose a coarse-fine-refine registration strategy for estimating 6-DoF pose between it and the query scan. This initially estimates a coarse pose by aligning the sparse matched node centers. Then, a fine registration of dense instance points is applied. Additional planar information from the background points further refines the final pose estimation using point-to-plane constraints. This strategy aligns both foreground instances and background points, with each stage starting from a favorable initial value, ensuring accuracy and efficiency. Fig. 1 illustrates how our method accurately detects loop closures and identifies instance node correspondences, even in places with significant direction and position differences, thus finally estimating the loop pose and closing the loop.

In summary, our contributions are fourfold: (i) We propose a novel semantic graph-guided full loop closing framework, SGLC, that offers robust loop detection and accurate 6-DoF pose estimation. (ii) We design an effective and efficient outlier pruning method to remove incorrect node correspondences. (iii) We proposed a coarse-fine-refine registration scheme that improves the accuracy and efficiency of pose estimation. (iv) We seamlessly incorporate SGLC into a current SLAM framework, reducing the error in odometry estimations. Extensive evaluation results on KITTI [15] and KITTI-360 [16] datasets support these claims.

II. RELATED WORK

Handcrafted-based approaches. These methods typically utilize the geometric features within the point cloud to describe it. In the early stages, Magnusson et al. [17] explore the application of the Normal Distributions Transform (NDT) for surface representation to develop histogram descriptors based on surface orientation and smoothness. The descriptors perform well in different environments and provide the inspiration for subsequent NDT-based methods [18], [19]. To quickly extract descriptors, some methods project point clouds into 2D plane [1], [4], [7], [8], [10] for encoding features. Among them, Scan Context (SC) family [4], [7], [10] is widely used due to its high efficiency and good LCD performance. It converts the raw point cloud into a polar coordinate bird’s eye view (BEV) and encodes the maximum height into the image bins. This yields rotation-invariant ring key descriptors for retrieval and a more detailed 2D image matrix for calculating similarity. Based on that, Wang et al. [4] argue that intensity information of point cloud is effective for loop closing, so they encode the intensity property into SC. Recently, Cui et al. [12] propose BoW3D, a bag of words (BoW)-based method leveraging Link3D features [20], which not only has robust LCD capability but also can estimate 6-DoF pose.

DNN-based approaches. Deep Neural Networks (DNN)-based methods commonly leverage deep neural networks to extract local features and then aggregate them into a global descriptor for retrieval. The early DNN-based work PointNetVLAD [2] is a combination of PointNet [21] for extracting

features and NetVLAD [22] for generating the final descriptor. After this, a variety of learning-based loop closing methods begin to proliferate. Liu et al. [23] proposed an adaptive feature extraction module and a graph-based neighborhood aggregation module for enhancing PointNetVLAD. In contrast to them, Komorowski et al. [24] build a sparse voxelized point cloud representation and extract features by sparse 3D convolutions. Chen et al. [9] propose OverlapNet, a range image-based LCD method by estimating image overlap. A subsequent enhanced version, OverlapTransformer [5] is proposed with superior performance and higher efficiency. Cattaneo et al. [11] proposed LCDNet, a robust LCD and 6-DoF pose estimation network validated in various environments, but its high computational complexity makes real-time running challenging. Recently, Luo et al. [6] proposed a lightweight BEV-based NetVALD [22] network that exhibits high descriptor generation efficiency and LCD capability. However, its descriptor dimension far exceeds others, leading to substantial storage consumption, particularly for robots only equipped with low-cost microcontrollers.

Some methods also incorporate semantic information to enhance the descriptor distinctiveness. Kong et al. [3] and Zhu et al. [14] attempt to build semantic graphs for loop closing, while Li et al. [10] utilize semantics to improve existing descriptors. We also believe semantics are helpful for loop closing as they distinguish different objects in the scene beforehand. However, few semantic-based methods work efficiently and effectively for 6-DoF loop closing.

III. SEMANTIC GRAPH-GUIDED LOOP CLOSING

This section details our semantic graph-guided loop closing approach, dubbed SGLC shown in Fig. 2, which includes building graphs from the raw point clouds (Sec. III-A), LiDAR scan descriptor generation (Sec. III-B), geometric verification (Sec. III-C) and pose estimation (Sec. III-D).

A. Semantic Graph

Semantic graph is a fundamental component of our SGLC, which generates distinctive descriptors and guides the subsequent geometric verification and pose estimation. Given a raw LiDAR scan \mathcal{S} , semantic label for each point can be obtained using an existing semantic segmentation method [25] with the ability to distinguish between moving and static objects. We then apply clustering [26] to such semantic point clouds to identify object instances. Subsequently, the bounding box of instances can be estimated by enclosing these clusters. As foreground instances such as *pole* and *trunk* are naturally standalone, they can be easily represented as individual nodes in the graph. Background point clouds, such as *building* and *fence*, typically have extensive points and are viewpoint-dependent, making them unstable for representation as instance nodes. Therefore, we construct semantic graphs only for stable foreground instances, such as *pole*, *trunk*, *lamp*, *static vehicle*. Each node \mathbf{v} comprises instance center position $\mathbf{c} = [x, y, z]^T$, bounding box size $\mathbf{b} = [l, h, w]$, a semantic label l_v , and a node descriptor $\mathbf{f} \in \mathbb{R}^D$ generated based on the semantic graph typologies.

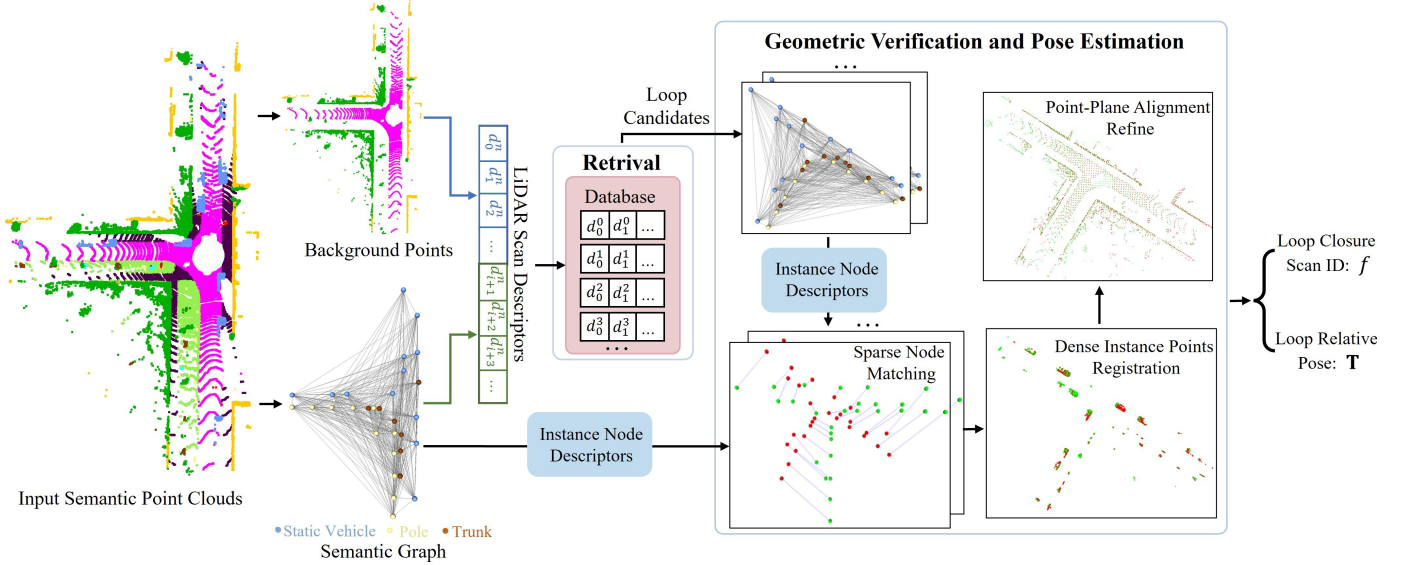


Fig. 2: The framework of SGLC. It first builds a semantic graph for foreground instances and then generates LiDAR scan descriptor considering both the topological properties of the semantic graph and the appearance characteristics of the background. The LiDAR scan descriptor is utilized to retrieve loop candidate scans from the database. Following this, geometric verification is performed on each loop candidate to filter out false loop closure, with the key step utilizing the instance node descriptors for robust sparse node matching. Finally, a coarse-fine-refine registration scheme is employed to estimate the precise 6-DoF pose.

Graph edges are established between pairs of nodes if their spatial Euclidean distance is less than d_{\max} . Each edge $e = (\mathbf{v}_i, \mathbf{v}_j)$ is described by a label l_e determined by the two nodes it connects and the length d . The label l_e include categories such as *pole-lamp*, *pole-trunk*, and so on. Finally, we obtain the semantic graph \mathcal{G} with a set of nodes \mathcal{V} and a set of edges \mathcal{E} . The graph adjacency matrix $\mathbf{A} \in \mathbb{R}^{N \times N}$ is created as:

$$\mathbf{A}_{ij} = \begin{cases} 1 & \text{if } (\mathbf{v}_i, \mathbf{v}_j) \in \mathcal{E}, \\ 0 & \text{otherwise} \end{cases} \quad (1)$$

where N is the number of nodes.

Based on the semantic graph, we design the distinctive instance node descriptor for each node, which is utilized for the subsequent robust node matching. We first encode the local relationships of nodes, which can be captured by edges connected to themselves. So we categorize and quantify all edges connected to each node, thereby constructing a histogram-based descriptor. Specifically, for a node $\mathbf{v} \in \mathcal{V}$, we categorize all connected edges into different intervals based on their labels and lengths, and count the occurrences within each interval to generate the descriptor \mathbf{f}_l .

Due to the \mathbf{f}_l only capturing the local typologies within the node neighborhood, it does not account for each node's global properties, such as their global centrality. To enhance the distinctiveness of the descriptor for robust node matching, we employ eigenvalue decomposition on the graph adjacency matrix \mathbf{A} , yielding $\mathbf{A} = \mathbf{Q}\mathbf{\Lambda}\mathbf{Q}^T$. The eigenvalues in $\text{diag}(\mathbf{\Lambda}) = \lambda_1, \dots, \lambda_n$ are arranged in descending order. The i -th row of \mathbf{Q} represents the i -th instance node embeddings, which capture the node's global properties in the graph [27]. Therefore, we use the each row of \mathbf{Q} as part of the instance node descriptor. Considering that the dimensions of the matrix \mathbf{Q} generated by each graph are different, and to unify dimensions of the descriptor, we encode each node using the first k columns

of \mathbf{Q} , i.e., the eigenvectors corresponding to the largest k eigenvalues, thereby generating a row vector $\mathbf{f}_g \in \mathbb{R}^k$ for each node. Note that the signs of eigenvectors are arbitrary, hence we use their absolute values. Finally, by concatenating $\mathbf{f}_l, \mathbf{f}_g$, we obtain each instance node's descriptor $\mathbf{f} \in \mathbb{R}^D$ in the graph.

B. LiDAR Scan Descriptor for Retrieval

Based on our devised semantic graph, we can effectively detect the loop closure. Theoretically, we could use local node descriptors to determine graph similarity and find loops directly. However, graph matching using nodes for LCD on a scan-scan basis is highly time-consuming, making it unsuitable for real-time SLAM systems. For fast loop candidate retrieving, we design a novel global descriptor for each LiDAR scan, including the foreground descriptor \mathbf{F}_f and background descriptor \mathbf{F}_b .

We generate \mathbf{F}_f based on our proposed foreground semantic graph, using the graph edges and nodes. The first part of \mathbf{F}_f is similar to the first part of node descriptor \mathbf{f}_l as an edge-based histogram descriptor. Instead of considering only the edges connected to a particular node, for \mathbf{F}_f , we account for all edges within the entire graph. These edges are categorized into subintervals in the histogram based on their types and lengths, forming the global edge descriptor. For the second part, We tally the number of nodes with different labels in the semantic graph to effectively describe the node distribution.

Besides \mathbf{F}_f , which captures the topological relationships between foreground instances, we further design a descriptor to exploit the extensive geometric information in the background point clouds. Inspired by Scan Context [7] encoding the maximum height of the raw point cloud into different bins of a polar BEV image, we leverage semantic information to replace the height data, constructing similar descriptors based on the background point cloud to generate rotation-invariant

ring key descriptors. It efficiently encodes the appearance characteristics of different background point clouds, offering a concise portrayal at a minimal computational cost.

Finally, we normalize \mathbf{F}_f and \mathbf{F}_b , and concatenate them to form the LiDAR scan descriptor $\mathbf{F} \in \mathbb{R}^{D'}$. This comprehensive descriptor incorporates features from both the foreground semantic graph and the background, thus possessing stronger retrieval capabilities. The LiDAR scan descriptor is utilized to retrieve the multiple similar candidate scans in the database. The similarity between descriptors is computed using the Euclidean distance within the feature space. In real applications, we use the FAISS library [28] to establish the descriptors database and perform fast parallel retrieving.

C. Geometric Verification

Once loop candidates are obtained, geometric verification is performed on each candidate to determine whether a true loop closure has occurred. The core of geometric verification is to establish node correspondences and estimate an initial relative pose between the query and candidate scans. The similarity between them is then measured by assessing the degree of alignment, including the following four steps:

Instance Nodes Matching. For the query scan with semantic graph \mathcal{G}_q and the target candidate scan with semantic graph \mathcal{G}_t , we create an affiliation matrix $\mathbf{I} \in \mathbb{R}^{N \times M}$ based on node descriptor similarity, where N and M are the number of nodes in the query and target graphs, respectively. Each element in \mathbf{I} is calculated as:

$$\mathbf{I}_{ij} = \begin{cases} 1 - \frac{\mathbf{f}_i^q \cdot \mathbf{f}_j^t}{\|\mathbf{f}_i^q\| \times \|\mathbf{f}_j^t\|} & \text{if } l_{vi}^q = l_{vj}^t \text{ and } \mathbf{b}_i^q = \mathbf{b}_j^t, \\ 10^8 & \text{otherwise} \end{cases} \quad (2)$$

\mathbf{I}_{ij} denotes the cost of assigning the i -th node in \mathcal{G}_q to the j -th node in \mathcal{G}_t . A high cost is assigned to reject a match if their node labels are inconsistent or bounding box sizes differ significantly.

The matching results are then determined using the Hungarian algorithm [29], yielding the instance node matching correspondence set between \mathcal{G}_q and \mathcal{G}_t as:

$$\mathcal{M}_q = \{\mathbf{c}_1^q, \mathbf{c}_2^q, \dots, \mathbf{c}_o^q\}, \quad (3)$$

$$\mathcal{M}_t = \{\mathbf{c}_1^t, \mathbf{c}_2^t, \dots, \mathbf{c}_o^t\}, \quad (4)$$

where $\mathbf{c} = [x, y, z]^T$ is the position of node mentioned earlier, o is the number of node matching pairs.

Node Correspondences Pruning. Due to changes in viewpoint during revisit or errors in semantic segmentation, there are incorrect node correspondences. Although RANdom SAMple Consensus (RANSAC) [30] can exclude some outliers, using it with all node matches substantially increases the number of iterations, making it unsuitable for online applications.

To reduce the computational complexity, we propose an efficient outlier pruning scheme based on the local structure of nodes before applying RANSAC. We posit that two nodes of a true positive correspondence should exhibit consistent local geometric structures. For a node \mathbf{v} , its neighboring nodes within a certain range can be represented as $\{\mathbf{v}_j\}_{j=1}^K$, where

K is the total number of neighbors. \mathbf{v} and any two of its neighbors can form a triangle, denoted as Δ_j , and all local triangles of \mathbf{v} is $\{\Delta_j\}_{j=1}^{K(K-1)/2}$. In an ideal scenario, corresponding local geometric triangles of matched nodes should be perfectly aligned. However, practical applications are subject to errors from semantic segmentation and clustering. Therefore, we relax this condition to prevent the elimination of correct correspondences. For the matching of local triangles, we consider two triangles to be consistent when their corresponding sides are of equal length. By doing so, we can effectively eliminate the false node correspondences.

Initial Pose Estimation. Based on pruned correspondences, denoted as \mathcal{M}'_q and \mathcal{M}'_t , we can efficiently estimate a relative pose between the query scan and candidate scan based on RANSAC and SVD decomposition [31]. Specifically, in each RANSAC iteration, we randomly select three matching pairs of \mathcal{M}'_q and \mathcal{M}'_t to solve the transformation equation based on SVD decomposition as:

$$\mathbf{R}_i, \mathbf{t}_i = \min_{\mathbf{R}, \mathbf{t}} \sum_{j=1}^3 \|\mathbf{R} \cdot \mathbf{c}_j^t + \mathbf{t} - \mathbf{c}_j^q\|_2^2, \quad (5)$$

by which we obtain a transformation in each iteration and finally select the transformation with the greatest number of inliers from all iterations as a coarse pose estimation for loop candidate verification $\mathbf{T}_{\text{coarse}} = \{\mathbf{R}_c, \mathbf{t}_c\}$.

Loop Candidate Verification. We verify the loop candidates by calculating scan similarity on two levels. First, we evaluate the semantic graph similarity between the query scan and candidate scan as follows:

$$S_{\text{graph}} = \exp\left(-\frac{\sum_{j=1}^u \|\mathbf{R}_c \cdot \mathbf{c}_j^{t'} + \mathbf{t}_c - \mathbf{c}_j^{q'}\|_2}{u}\right), \quad (6)$$

where $\mathbf{c}_j^{t'}$, $\mathbf{c}_j^{q'}$ are the inlier correspondences. u is the number of inliers. S_{graph} measures the alignment of the two graphs.

Furthermore, we utilize $\mathbf{T}_{\text{coarse}}$ to align the background point clouds of the query scan and candidate scan, and then calculate the cosine similarity of their background descriptors \mathbf{F}_b^q and \mathbf{F}_b^t . This additional term provides greater reliability compared to using graph similarity alone. If both S_{graph} and the background similarity exceed their respective thresholds, the query scan and the candidate scan are considered a true loop closure. We then proceed to estimate their precise pose transformation as follows.

D. 6-DoF Pose Refinement

The aforementioned $\mathbf{T}_{\text{coarse}}$, estimated at the sparse instance node level, may not be accurate and robust enough for closing the loop. To enhance the accuracy of the relative pose estimation, we propose performing a dense points registration on all foreground instance points from the input semantic point cloud, using $\mathbf{T}_{\text{coarse}}$ as the initial transformation.

Benefiting from the already obtained instance node matches, finding the corresponding point matches between matched instances becomes easy and fast due to the significantly reduced search space. In fact, $\mathbf{T}_{\text{coarse}}$ already initially align the query scan and candidate scan. Therefore, directly searching

for the nearest neighbor points as point matches is sufficient to initialize and solve the Iterative Closest Point (ICP) as:

$$\mathbf{T}_{\text{icp}} = \min_{\mathbf{T}} \sum_{(\mathbf{p}_j^q, \mathbf{p}_j^t) \in \mathcal{C}} \|\mathbf{T}\mathbf{p}_j^t - \mathbf{p}_j^q\|_2^2, \quad (7)$$

where \mathcal{C} is the set of instance points nearest neighbor correspondences between query scan and loop scan.

The dense registration result \mathbf{T}_{icp} encompasses the registration of all foreground instance points. However, background points, such as those from buildings and roads offering stable plane features, are also valuable for pose estimation. Therefore, to further optimize the pose accuracy from dense points registration, we utilize point-to-plane residuals to refine the final relative pose.

$$\mathbf{T}_{\text{refine}} = \min_{\mathbf{T}} \sum_{(\mathbf{p}_j^{q'}, \mathbf{p}_j^{t'}) \in \mathcal{C}'} \|\mathbf{n}_j^{\top} (\mathbf{T}\mathbf{p}_j^{t'} - \mathbf{p}_j^{q'})\|_2^2, \quad (8)$$

where \mathcal{C}' is the set of point correspondences with consistent plane normal vector, denoted as $\mathbf{n}_j^{\top} \in \mathbb{R}^3$.

$\mathbf{T}_{\text{coarse}}$ is estimated via sparse graph node matching, while \mathbf{T}_{icp} is determined by dense instance point registration. This sparse-to-dense registration mechanism enhances pose estimation accuracy in a coarse-to-fine manner. Finally, the relative pose is further refined using point-to-plane constraints for background points. This semantically-guided coarse-fine-refine pose estimation process considers the alignment of both instance points and background points. By separately handling instance points and background points, each alignment stage begins with a favorable initial value, ensuring fast matching and convergence, as well as multi-step checked robust pose estimation.

IV. EXPERIMENTAL EVALUATION

A. Experimental Setup

Dataset. We evaluate our method on two publicly available datasets: KITTI [15] and KITTI-360 [16]. KITTI includes 11 sequences with ground truth poses, among which six sequences (00, 02, 05, 06, 07, 08) contain loop closures and sequence 08 contains reverse loop closures. KITTI-360 is composed of 9 sequences, with 6 of them containing loops. Compared to KITTI, KITTI-360 has a greater number of loop closures and reverse loop closures.

Implement Details. In our experiments, we set $d_{\text{max}} = 60$, $k = 30$, and the graph and background similarity thresholds are 0.58 and 0.7, respectively. We use the semantic information from a semantic segmentation network [25] on both datasets and mainly build semantic graphs from *static vehicle*, *pole* and *trunk* instances, and utilize background points from *building*, *fence*, *road* and *vegetation*. This is convenient for replacing or adding other semantic information. All the experiments are conducted on a machine with an AMD 3960X @3.8GHz CPU and a NVIDIA RTX 3090 GPU. More implementation details can be found in our open-source repository.

B. Loop Closure Detection

We follow the experimental setups of Li et al. [10] to evaluate loop closure detection performance. For the KITTI

dataset, we perform performance comparisons on all sequences with loop closure. For the KITTI-360 dataset, in line with [11], we focus on evaluation sequences 0002 and 0009 with the highest number of loop closures. In the experiments, we regard LiDAR scan pairs as positive samples of loop closure when their Euclidean distance is less than 3 m and as negative samples if the distance exceeds 20 m.

Metrics. Following [10], [12], we use the maximum F_1 score and Extended Precision (EP) as evaluation metric:

$$F_1 = 2 \times \frac{P \times R}{P + R} \quad (9)$$

$$EP = \frac{1}{2}(P_{R0} + R_{P100}) \quad (10)$$

where P, R denote the precision and recall, respectively. P_{R0} is the precision at minimum recall and R_{P100} the max recall at 100% precision.

Baselines. We compare the results with SOTA baseline methods, including DNN-based methods: PointNetVLAD [2], OverlapNet [9], LCDNet [11], OverlapTransformer (OT) [5], BEVPlace [6], as well as handcrafted-based methods: Scan Context [7], LiDAR-Iris [8], GOSMatch [14], SSC [10], BoW3D [12].

Results. The results are shown in Tab. I. Our method outperforms SOTA on multiple sequences and achieves the best average F1max score and EP for the KITTI dataset. Specifically, for sequence 08 which only contains reverse loop closure, our approach still exhibits superior performance while most handcrafted-based methods suffer from significant degradation. This proves that our method possesses good rotational invariance. For the KITTI-360 dataset, our method can still get competitive results, demonstrating its generalization capability.

Furthermore, to investigate the loop closure detection performance at further distances, we followed [5], [9] to regard two LiDAR scans as a loop closure when their overlap ratio is beyond 0.3, which indicates that the maximum possible distance between them is around 15 m. We adopt the same experimental setup as theirs to evaluate our method on the KITTI 00 sequence using AUC, F1max, Recall@1, and Recall@1% as metrics. The results are shown in Tab. II. Due to BoW3D leaning more towards geometric verification, we are unable to generate its AUC and recall@1% results from its open-source implementation. From the results, our method significantly outperforms SOTA baselines in terms of overall metric, indicating its robustness for detecting long-distance loop closures. Although GOSMatch also has a commendable recall capability, its F1max score is slightly inferior to other methods, indicating an insufficient capability to accurately determine true loop closure.

C. Loop Pose Estimation

To validate the loop pose estimation performance, we follow Cattaneo et al. [11] and evaluate our approach on the sequences 00 and 08 of the KITTI dataset, sequences 0002 and 0009 of the KITTI-360 dataset. To keep consistent with them, we choose the loop closure samples when the distance is within 4 m. Additionally, we also select the more challenging closed-loop pairs with low overlap for testing.

TABLE I: The performance comparison of F1 max scores and Extended Precision on the KITTI and KITTI-360 datasets.

Methods	KITTI							KITTI-360		
	00	02	05	06	07	08	Mean	0002	0009	
DNN-based	PointNetVLAD	0.779/0.641	0.727/0.691	0.541/0.536	0.852/0.767	0.631/0.591	0.037/0.500	0.595/0.621	0.349/0.515	0.330/0.510
	OverlapNet	0.869/0.555	0.827/0.639	0.924/0.796	0.930/0.744	0.818/0.586	0.374/0.500	0.790/0.637	0.308/0.527	0.739/0.605
	LCDNet	0.970/0.847	0.966/0.917	0.969/0.938	0.958/0.920	0.916/0.684	0.989/0.908	0.961/0.869	0.998/0.993	0.988/0.734
	OT	0.873/0.800	0.810/0.725	0.837/0.772	0.876/0.809	0.625/0.505	0.667/0.510	0.781/0.687	0.796/0.507	0.879/0.528
	BEVPlace	0.960/0.849	0.845/0.819	0.885/0.815	0.895/0.815	0.917/0.687	0.967/0.868	0.912/0.809	0.920/0.504	0.938/0.684
Handcrafted	Scan Context	0.750/0.609	0.782/0.632	0.895/0.797	0.968/0.924	0.662/0.554	0.607/0.569	0.777/0.681	0.771/0.554	0.851/0.619
	LiDAR-Iris	0.668/0.626	0.762/0.666	0.768/0.747	0.913/0.791	0.629/0.651	0.478/0.562	0.703/0.674	0.704/0.552	0.782/0.580
	GOSMatch	0.927/0.651	0.720/0.500	0.840/0.612	0.518/0.521	<u>0.939/0.879</u>	0.908/0.571	0.809/0.622	0.694/0.500	0.766/0.575
	SSC	0.939/0.826	<u>0.890/0.745</u>	0.941/0.900	<u>0.986/0.973</u>	<u>0.870/0.773</u>	0.881/0.732	0.918/0.825	<u>0.974/0.780</u>	0.970/0.866
	BoW3D	<u>0.977/0.981</u>	0.578/0.704	<u>0.965/0.969</u>	<u>0.985/0.985</u>	<u>0.906/0.929</u>	0.900/0.866	<u>0.885/0.906</u>	0.210/0.560	0.682/0.761
Ours	0.999/0.984	0.888/ <u>0.899</u>	0.971/0.972	0.995/0.970	0.998/0.994	<u>0.988/0.980</u>	0.973/0.967	0.932/ <u>0.934</u>	0.994/0.978	

[F_1 max / EP], the best scores are highlighted in bold and the second scores are underlined.

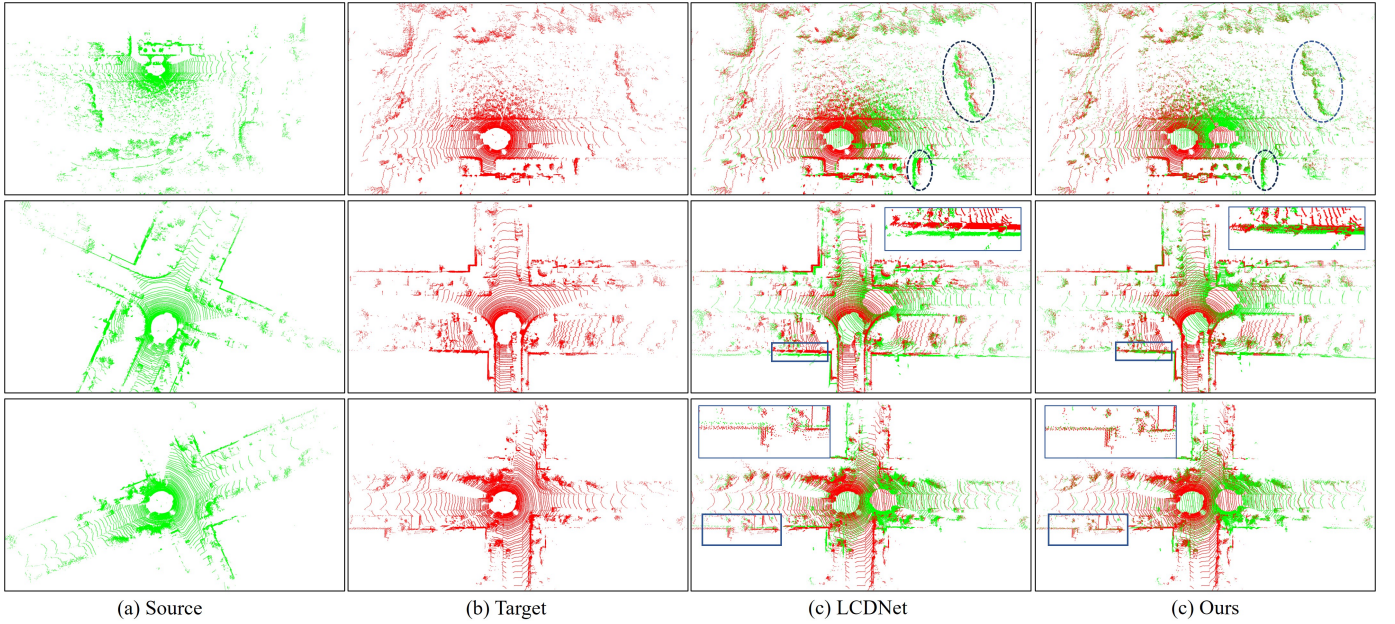


Fig. 3: The qualitative comparison of loop pose estimation on the KITTI dataset using overlap-based loop pairs. Dashed ellipses are directly annotated on the registration results, while solid boxes indicate local magnification.

TABLE II: The performance evaluation of loop closure detection on the KITTI dataset using overlap-based loop pairs.

Methods	AUC	F1max	Recall @1	Recall @1%	
	DNN-based	PointNetVLAD	0.856	0.846	0.776
OverlapNet		0.867	0.865	0.816	0.908
LCDNet		0.933	0.883	0.915	0.974
OT		0.907	0.877	0.906	0.964
BEVPlace		0.926	0.889	0.913	0.972
Handcrafted	Scan Context	0.836	0.835	0.820	0.869
	LiDAR-Iris	0.843	0.848	0.835	0.877
	GOSMatch	0.926	0.844	<u>0.945</u>	1.0
	SSC	<u>0.937</u>	<u>0.913</u>	0.906	0.959
	BoW3D	-	0.893	0.807	-
Ours	0.953	0.934	0.957	<u>0.989</u>	

The best results are highlighted in bold and the second results are underlined.

Metric. We apply three evaluation metrics for comparisons:

(i) Registration Recall (RR): represents the percentage of successful alignment. (ii) Relative Translation Error (RTE),

the Euclidean distance between the ground truth and estimated poses. (iii) Relative Yaw Error (RYE), the yaw angle difference between the ground truth and estimated poses. Two scans are regarded as a successful registration when the RTE and RYE are below 2 m and 5° , respectively.

Baselines. The baseline methods for comparison mainly include 6-DoF pose estimation methods BoW3D [12] and LCDNet [11]. LCDNet is available in two version: LCDNet (fast) utilizes an unbalanced optimal transport (UOT)-based head to estimate relative pose while LCDNet replaces the head by a RANSAC estimator.

Results. As shown on the left of Tab. III, our method achieves competitive results compared to LCDNet, and exceeds LCDNet (fast) and BoW3D by a large margin on the KITTI dataset of the closed loop within 4 meters. Both in the same direction loop correction in sequence 00 and reverse loop correction in sequence 08, our method and LCDNet get a high registration recall (RR) while BoW3D and LCDNet (fast) degrade significantly in reverse loop correction. In terms of RTE,

TABLE III: The comparison of loop pose estimation errors on the KITTI dataset

	<i>Distance – based closed loop</i>						<i>Overlap – based closed loop</i>						Time(ms)
	Seq.00			Seq.08			Seq.00			Seq.08			
	RR(%)	RTE(m)	RYE(°)	RR(%)	RTE(m)	RYE(°)	RR(%)	RTE(m)	RYE(°)	RR(%)	RTE(m)	RYE(°)	
BoW3D	95.50	<u>0.06</u>	0.84	77.36	<u>0.09</u>	2.01	57.02	<u>0.07</u>	0.96	47.21	<u>0.10</u>	1.93	<u>118.1</u>
LCDNet(fast)	93.03	0.65	0.86	60.71	1.02	1.65	66.82	0.56	0.68	47.29	0.88	1.06	229.3
LCDNet	100	0.11	0.12	100	0.15	0.34	<u>94.86</u>	0.23	<u>0.24</u>	<u>96.87</u>	0.31	<u>0.51</u>	576.7
Ours	100	0.04	<u>0.18</u>	100	0.07	<u>0.39</u>	99.94	0.04	0.19	99.60	0.07	0.40	97.3*

* denotes the entire runtime including the semantic segmentation. The best results are highlighted in bold and the second results are underlined.

TABLE IV: The comparison of loop pose estimation errors on the KITTI-360 dataset.

	Seq.0002			Seq.0009			Time (ms)
	RR(%)	RTE(m)	RYE(°)	RR(%)	RTE(m)	RYE(°)	
BoW3D	67.62	0.19	2.03	87.40	<u>0.13</u>	1.27	120.8
LCDNet(fast)	82.92	0.84	1.28	89.49	0.76	0.99	254.4
LCDNet	98.62	0.28	0.32	100	0.18	0.20	627.9
Ours	<u>95.14</u>	<u>0.20</u>	<u>0.85</u>	<u>99.87</u>	0.11	<u>0.48</u>	98.9*

* denotes the entire runtime including the semantic segmentation. The best results are highlighted in bold and the second results are underlined.

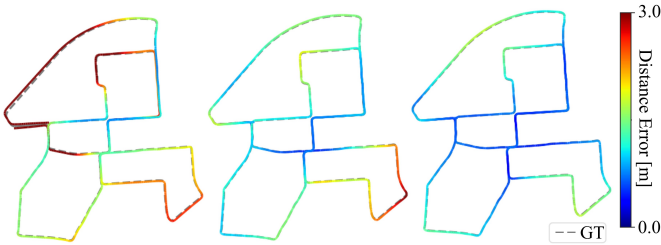


Fig. 4: The trajectory of A-LOAM odometry (left) compared to with integrating BoW3D loop closing method (middle) and integrating our approach (right) on the KITTI 00 sequence.

our method excels over LCDNet, demonstrating its superior performance in translation estimation. To further highlight the gap between these methods, we test them on loop pairs with an overlap ratio exceeding 0.3. The comparison results are presented on the right of Tab. III. It can be seen that our method still maintains strong registration performance and surpasses all others across all metrics, emphasizing its robustness. In comparison, LCDNet experienced a performance decline when performing registration with low overlap. We also present the qualitative results in Fig. 3. As can be seen, our method achieves better alignment even in low overlap loop closure, attributing to the semantically-guided coarse-fine-refine point cloud alignment process. Tab. IV shows the results on the KITTI-360 dataset with close loop within 4 m. We also report the average running time for all methods on our machine. From the registration results, our method remains competitive compared to other baselines, demonstrating the generalizability of our approach. Additionally, our method achieves the fastest running speed and significantly outperforms other methods even when the time of semantic segmentation is included, approximately 67.1 ms for SegNet4D [25]. By comparison, LCDNet operates with extreme time consumption, rendering it unsuitable for real-time SLAM systems.

TABLE V: Ablation studies on KITTI 08 sequence. “Node Glo.” denotes the global properties of instance node, mentioned in Sec. III-A. “Out. Pru.” denotes outlier pruning for node correspondences. “Den. ICP” denotes dense points registration, i.e., T_{icp} . “P-P Ali.” denotes point-plane alignment, i.e., T_{refine} .

	Node Glo.	Out. Pru.	Den. ICP	P-P Ali.	F1max	RR(%)	RTE(m)	RYE(°)	Time (ms)
[A]					0.981	97.20	0.23	1.31	10.2
[B]	✓				0.987	97.80	0.22	1.29	+0.6
[C]	✓	✓			0.988	98.61	0.20	0.98	+1.4
[D]	✓	✓	✓		-	99.97	0.08	0.50	+13.2
[E]	✓	✓		✓	-	99.53	0.08	0.42	+7.9
[F]	✓	✓	✓	✓	-	100	0.07	0.39	+21.8

“+” denotes the time increment compared to [A]. The best results are highlighted in bold

D. Performance on SLAM System

We integrate our method into the A-LOAM odometry to eliminate cumulative errors for evaluating the accuracy of SLAM trajectories, and compare the results with baseline integrated with BoW3D. We utilize a Incremental Smoothing and Mapping (iSAM2) [32] based pose-graph optimization (PGO)¹ framework to build a factor graph for managing the the keyframe poses. If a loop closure is detected, we will add this loop closure constraint into the factor graph to eliminate errors and ensure global consistency. As shown in Fig. 4, we present the trajectory error analysis between keyframe and ground truth poses. From the results, our method significantly enhances the SLAM system by reducing the cumulative odometry error, and shows superior performance compared to the baseline that incorporates BoW3D. This improvement is attributed to the excellent loop closing capability of our approach.

E. Ablation Study

In this section, we conduct a series of ablation studies to evaluate the effectiveness of designed components and analyze their runtime. The results are presented in Tab. V. The Experiment [A] is our baseline by removing those components listed in Tab. V. Comparing Experiment [A] and [B], it is demonstrated that incorporating the global properties of instance nodes can enhance the performance of loop closing. As anticipated, it increases each node’s distinctiveness, which is beneficial for finding the correct node correspondences. In Experiment [C], we can see the effectiveness of outlier pruning

¹<https://github.com/gisbi-kim/SC-A-LOAM>

in improving registration accuracy with the same number of RANSAC iterations as [B]. For Experiment [D], [E] and [F], dense points registration and point-plane alignment are applied mainly for loop scan determined after geometric verification, so they do not affect the results of loop closure detection. The results clearly show that both dense points registration and point-plane alignment can improve registration performance, and we can get optimal results only when they operate in conjunction. Besides, each component in our framework exhibits high execution efficiency from the runtime perspective.

V. CONCLUSION

This paper presents a semantic graph-guided approach for LiDAR-based loop closing. It initially builds a semantic graph of the foreground instances, which serves as the foundation for descriptor generation and guides subsequent steps in geometric verification and pose estimation. The designed LiDAR scan descriptor leverages both the semantic graph's topological properties and the appearance characteristics of the background point cloud, thereby enhancing its robustness in loop closure detection. For loop pose estimation, we proposed a coarse-fine-refine registration scheme that considers the alignment of both instance points and background points, offering high efficiency and accuracy. The proposed method supports real-time online operation and is convenient for integration into SLAM systems, particularly semantic SLAM. The experimental results on different datasets demonstrate its superiority.

REFERENCES

- [1] L. He, X. Wang, and H. Zhang. M2DP: A novel 3D point cloud descriptor and its application in loop closure detection. In *Proc. of the IEEE/RSJ Intl. Conf. on Intelligent Robots and Systems (IROS)*, 2016.
- [2] M. A. Uy and G. H. Lee. PointNetVLAD: Deep Point Cloud Based Retrieval for Large-Scale Place Recognition. In *Proc. of the IEEE/CVF Conf. on Computer Vision and Pattern Recognition (CVPR)*, 2018.
- [3] X. Kong, X. Yang, G. Zhai, X. Zhao, X. Zeng, M. Wang, Y. Liu, W. Li, and F. Wen. Semantic Graph Based Place Recognition for 3D Point Clouds. In *Proc. of the IEEE/RSJ Intl. Conf. on Intelligent Robots and Systems (IROS)*, 2020.
- [4] H. Wang, C. Wang, and L. Xie. Intensity Scan Context: Coding Intensity and Geometry Relations for Loop Closure Detection. In *Proc. of the IEEE Intl. Conf. on Robotics & Automation (ICRA)*, 2020.
- [5] J. Ma, J. Zhang, J. Xu, R. Ai, W. Gu, and X. Chen. OverlapTransformer: An Efficient and Yaw-Angle-Invariant Transformer Network for LiDAR-Based Place Recognition. *IEEE Robotics and Automation Letters (RA-L)*, 7(3):6958–6965, 2022.
- [6] L. Luo, S. Zheng, Y. Li, Y. Fan, B. Yu, S. Cao, and H. Shen. BEVPlace: Learning LiDAR-based Place Recognition using Bird's Eye View Images. In *Proc. of the IEEE/CVF Intl. Conf. on Computer Vision (ICCV)*, 2023.
- [7] G. Kim, S. Choi, and A. Kim. Scan Context++: Structural Place Recognition Robust to Rotation and Lateral Variations in Urban Environments. *IEEE Trans. on Robotics (TRO)*, 38(3):1856–1874, 2022.
- [8] Y. Wang, Z. Sun, C. Xu, S. Sarma, J. Yang, and H. Kong. LiDAR Iris for Loop-Closure Detection. In *Proc. of the IEEE/RSJ Intl. Conf. on Intelligent Robots and Systems (IROS)*, 2020.
- [9] X. Chen, T. Labe, A. Milioto, T. Rohling, J. Behley, and C. Stachniss. OverlapNet: A Siamese Network for Computing LiDAR Scan Similarity with Applications to Loop Closing and Localization. *Autonomous Robots*, 46:61–81, 2021.
- [10] L. Li, X. Kong, X. Zhao, T. Huang, W. Li, F. Wen, H. Zhang, and Y. Liu. SSC: Semantic Scan Context for Large-Scale Place Recognition. In *Proc. of the IEEE/RSJ Intl. Conf. on Intelligent Robots and Systems (IROS)*, 2021.
- [11] D. Cattaneo, M. Vaghi, and A. Valada. LCDNet: Deep Loop Closure Detection and Point Cloud Registration for LiDAR SLAM. *IEEE Trans. on Robotics (TRO)*, 38(4):2074–2093, 2022.
- [12] Y. Cui, Y. Zhang, X. Chen, J. Dong, Q. Wu, and F. Zhu. BoW3D: Bag of Words for Real-Time Loop Closing in 3D LiDAR SLAM. *IEEE Robotics and Automation Letters (RA-L)*, 8:2828–2835, 2022.
- [13] Z. Qiao, Z. Yu, H. Yin, and S. Shen. Pyramid Semantic Graph-Based Global Point Cloud Registration with Low Overlap. In *Proc. of the IEEE/RSJ Intl. Conf. on Intelligent Robots and Systems (IROS)*, 2023.
- [14] Y. Zhu, Y. Ma, L. Chen, C. Liu, M. Ye, and L. Li. GOSMatch: Graph-of-Semantics Matching for Detecting Loop Closures in 3D LiDAR data. In *Proc. of the IEEE/RSJ Intl. Conf. on Intelligent Robots and Systems (IROS)*, 2020.
- [15] A. Geiger, P. Lenz, C. Stiller, and R. Urtasun. Vision meets Robotics: The KITTI Dataset. *Intl. Journal of Robotics Research (IJRR)*, 32:1231 – 1237, 2013.
- [16] Y. Liao, J. Xie, and A. Geiger. KITTI-360: A Novel Dataset and Benchmarks for Urban Scene Understanding in 2D and 3D. *IEEE Trans. on Pattern Analysis and Machine Intelligence (TPAMI)*, 45(3), 2023.
- [17] M. Magnusson, H. Andreasson, A. Nuchter, and A. J. Lilienthal. Appearance-Based Loop Closure from 3D Laser Data Using the Normal Distributions Transform. In *Proc. of the IEEE Intl. Conf. on Robotics & Automation (ICRA)*, 2009.
- [18] A. Zaganidis, A. Zernitev, T. Duckett, and G. Cielniak. Semantically Assisted Loop Closure in SLAM Using NDT Histograms. In *Proc. of the IEEE/RSJ Intl. Conf. on Intelligent Robots and Systems (IROS)*, 2019.
- [19] Z. Zhou, C. Zhao, D. Adolfsson, S. Su, Y. Gao, T. Duckett, and L. Sun. NDT-Transformer: Large-Scale 3D Point Cloud Localisation using the Normal Distribution Transform Representation. In *Proc. of the IEEE Intl. Conf. on Robotics & Automation (ICRA)*, 2021.
- [20] Yunge Cui, Yinlong Zhang, Jiahua Dong, Haibo Sun, Xieyuanli Chen, and Feng Zhu. Link3D: Linear Keypoints Representation for 3D LiDAR Point Cloud. *IEEE Robotics and Automation Letters (RA-L)*, 9(3):2128–2135, 2024.
- [21] C. R. Qi, H. Su, K. Mo, and L. J. Guibas. PointNet: Deep Learning on Point Sets for 3D Classification and Segmentation. In *Proc. of the IEEE Conf. on Computer Vision and Pattern Recognition (CVPR)*, 2017.
- [22] R. Arandjelovic, P. Gronat, A. Torii, T. Pajdla, and J. Sivic. NetVLAD: CNN Architecture for Weakly Supervised Place Recognition. In *Proc. of the IEEE Conf. on Computer Vision and Pattern Recognition (CVPR)*, 2016.
- [23] Z. Liu, S. Zhou, C. Suo, P. Yin, W. Chen, H. Wang, H. Li, and Y. Liu. LPD-Net: 3D Point Cloud Learning for Large-Scale Place Recognition and Environment Analysis. In *Proc. of the IEEE/CVF Intl. Conf. on Computer Vision (ICCV)*, 2019.
- [24] J. Komorowski. MinkLoc3D: Point Cloud Based Large-Scale Place Recognition. In *Proc. of the IEEE Winter Conf. on Applications of Computer Vision (WACV)*, 2021.
- [25] N. Wang, R. Guo, C. Shi, H. Zhang, H. Lu, Z. Zheng, and X. Chen. SegNet4D: Effective and Efficient 4D LiDAR Semantic Segmentation in Autonomous Driving Environments. *arXiv preprint*, 2024.
- [26] S. Park, S. Wang, H. Lim, and U. Kang. Curved-Voxel Clustering for Accurate Segmentation of 3D LiDAR Point Clouds with Real-Time Performance. In *Proc. of the IEEE/RSJ Intl. Conf. on Intelligent Robots and Systems (IROS)*, 2019.
- [27] G. Nikolentzos, P. Meladianos, and M. Vazirgiannis. Matching Node Embeddings for Graph Similarity. In *Proc. of the Conference on Advancements of Artificial Intelligence (AAAI)*, 2017.
- [28] J. Johnson, M. Douze, and H. Jégou. Billion-Scale Similarity Search with GPUs. *IEEE Transactions on Big Data*, 7:535–547, 2017.
- [29] H. W. Kuhn. The Hungarian Method for the Assignment Problem. *Naval Research Logistics (NRL)*, 52, 1955.
- [30] M. A. Fischler and R. C. Bolles. Random Sample Consensus: A Paradigm for Model Fitting with Applications to Image Analysis and Automated Cartography. *Communications of the ACM*, 24(6):381–395, 1981.
- [31] P. J. Besl and N. D. McKay. A Method for Registration of 3-D Shapes. *IEEE Trans. on Pattern Analysis and Machine Intelligence (TPAMI)*, 14(2):239–256, 1992.
- [32] M. Kaess, H. Johannsson, R. Roberts, V. Ila, J. J. Leonard, and F. Dellaert. iSAM2: Incremental smoothing and mapping using the Bayes tree. *Intl. Journal of Robotics Research (IJRR)*, 31:216 – 235, 2012.